NANO LETTERS

pubs.acs.org/NanoLett Letter

Greatly Enhanced Plasmon−Exciton Coupling in Si/WS_2/Au Nanocavities

Fu Deng,[§] Hongxin Huang,[§] Jing-Dong Chen, Shimei Liu, Huajian Pang, Xiaobing He, and Sheng Lan*

Cite This: *Nano Lett.* 2022, 22, 220−228 Read Online

ACCESS | Metrics & More | Article Recommendations | Supporting Information

ABSTRACT: A strong light−matter interaction is highly desirable from the viewpoint of both fundamental research and practical application. Here, we propose a dielectric−metal hybrid nanocavity composed of a silicon (Si) nanoparticle and a thin gold (Au) film and investigate numerically and experimentally the coupling between the plasmons supported by the nanocavity and the excitons in an embedded tungsten disulfide (WS_2) monolayer. When a Si/WS_2/Au nanocavity is excited by the surface plasmon polariton generated on the surface of the Au film, greatly enhanced plasmon−exciton coupling originating from the hybridization of the surface plasmon polariton, the mirror-image-induced magnetic dipole, and the exciton modes is clearly revealed in the angle- or size-resolved scattering spectra. A Rabi splitting as large as ∼240 meV is extracted by fitting the experimental data with a coupled harmonic oscillator model containing three oscillators. Our findings open new horizons for constructing nanoscale photonic devices by exploiting dielectric−metal hybrid nanocavities.

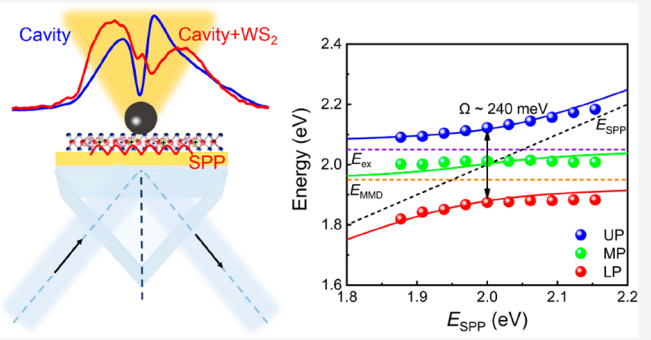

KEYWORDS: *dielectric nanoparticle, 2D material, dielectric−metal hybrid nanocavity, plasmon−exciton coupling*

Transition-metal dichalcogenide (TMDC) monolayers, which possess high optical absorption and large electric dipole moments,[1−7] have been widely employed for realizing strong light−matter interactions.[8−12] In these cases, mixed states known as polaritons are generated and the coupling strength is characterized by vacuum Rabi splitting.[9,13] Much attention has been paid to the strong-coupling regime, which exhibits potential applications in ultrafast optical switching,[14] quantum manipulation,[15] low-threshold lasing, etc.[16,17]

Recently, a strong coupling between the excitons in TMDC monolayers and the optical/plasmonic modes supported by optical microcavities[18,19] and metallic nanoparticles has been successfully demonstrated.[20−32] In addition, thermal tuning of plasmon−exciton coupling strength and the exciton oscillator strength was also realized.[33] Due to the small mode volumes of plasmonic resonators, Rabi splittings of 80−120 meV can be achieved.[21,23,24] To further enhance light−matter interactions, particle-on-film systems coupled with TMDC monolayers are employed, increasing Rabi splitting to 120−170 meV.[27−29]

In recent years, dielectric nanoparticles supporting Mie resonances were also employed to realize resonant coupling with TMDC monolayers. Recently, photon−exciton coupling approaching the strong-coupling regime has been demonstrated by using a silicon (Si) nanoparticle and a tungsten disulfide (WS_2) monolayer.[34,35] In this case, the energy transfer is mediated by the magnetic dipole (MD) resonance of the Si nanoparticle and the coupling strength can be modified by changing the surrounding environment.[34,35]

Basically, plasmonic nanocavities possess mode volumes much smaller than those of optical cavities, leading to a larger coupling strength. However, the heat originating from the Ohmic loss of plasmonic nanocavities at optical frequencies may affect the stability of two-dimensional TMDCs, preventing the investigation of temperature-sensitive phenomena. In previous studies, all-metallic particle-on-film systems (or nanocavities) were used to investigate strong plasmon−exciton coupling because a significant electric field enhancement is expected in the gap region. Unfortunately, it was found that the electric field in the gap region is dominated by the out-of-plane component in all-metallic nanocavities constructed with spherical nanoparticles.[36,37] The in-plane component of the electric field, which is crucial for coupling with the excitons in TMDC monolayers, is not enhanced as much (see Figure S1 in the Supporting Information). Since only electric dipoles (ED) can be excited in metallic nanoparticles, no Fano resonance (or dark mode) was observed when all-metallic nanocavities were excited by using surface plasmon polaritons (SPPs).[37,38] In comparison, dielectric−metal hybrid nanocavities have at-

Received: September 23, 2021
Revised: December 15, 2021
Published: December 28, 2021

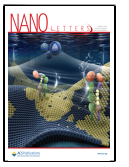

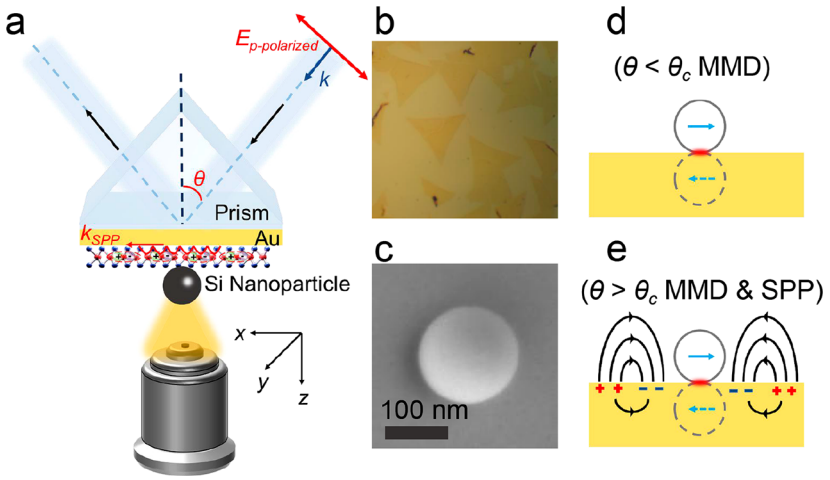

Figure 1. (a) Schematic showing the experimental setup used to investigate the plasmon−exciton coupling in a Si/WS_2/Au nanocavity. The Si/WS_2/Au nanocavity is excited by using *p*-polarized white light through a prism, and the scattering light is collected by using the objective of a microscope. (b) Optical image of WS_2 monolayers attached on the Au film. (c) SEM image of a typical Si nanoparticle with a spherical shape, which is employed to create a Si/Au or a Si/WS_2/Au nanocavity in this work. (d) Schematic showing the excitation of an ED in the Si nanoparticle and its mirror image induced by the Au film. (e) Schematic showing the simultaneous excitation of MMD and SSP in a Si/Au nanocavity by using a *p*-polarized plane wave with $\theta > \theta_c$.

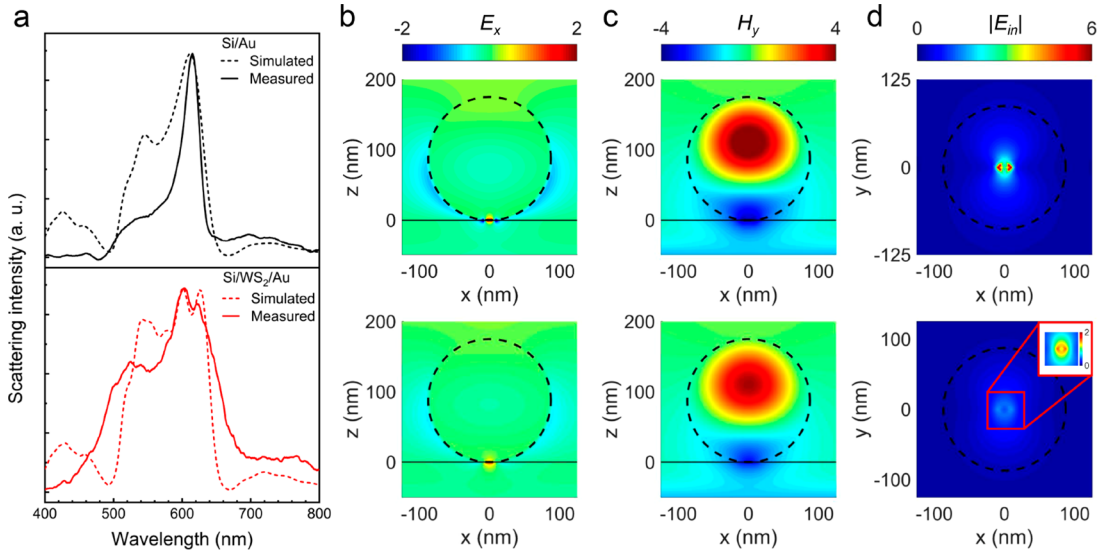

Figure 2. (a) Scattering spectra measured (solid curves) and simulated (dashed curves) for Si/Au (upper panel) and Si/WS_2/Au (lower panel) nanocavities. The electric (E_x, E_{in}) and magnetic (H_y) field distributions simulated for the two nanocavities at the exciton resonance (615 nm) in the *xz* and *xy* planes are shown in (b−d), respectively.

tracted great interest due to their ability to provide a strong localization of the electric field with suppressed Ohmic loss.[27−29,39] More importantly, both electric and magnetic dipoles can be simultaneously excited in a dielectric nanoparticle.[40,41] Consequently, a Fano resonance is generated in hybrid nanocavities when they are excited by SPPs, leading to a significant enhancement of the electric field, especially the in-plane component.[42]

In recent studies, the strong coupling of plasmons, excitons, and (microcavity) photons was demonstrated by introducing an external microcavity to enclose a plasmonic nanoparticle array on a TMDC monolayer, significantly enhancing the Rabi splitting energy.[19,43] It is noted, however, that the fabrication process of such a sample is very complicated, which may hinder practical applications. In addition, the tuning of the plasmon and photon modes was mainly achieved by modifying the geometrical parameters of the configuration, which may limit the manipulation of the coupling strength. On the other hand, it was predicted that a nonradiative (or "dark") mode can be used to boost the coupling of a nanocavity with quantum emitters.[44] It has been demonstrated that strong photon−exciton coupling with a Rabi splitting of ∼190 meV can be realized by exploiting the "anapole" formed in a single nanodisk made of TMDCs.[45,46] This finding reminds us that the dark mode involved in the Fano resonance, which was revealed in Si/Au hybrid nanocavities,[36] can be exploited to realize strong coupling with the WS_2 monolayer.

In this work, we investigate numerically and experimentally the plasmon−exciton coupling in Si/Au nanocavities with an embedded WS_2 monolayer and demonstrate greatly enhanced plasmon−exciton coupling with a Rabi splitting as large as ∼240 meV.

https://doi.org/10.1021/acs.nanolett.1c03576
Nano Lett. 2022, 22, 220−228

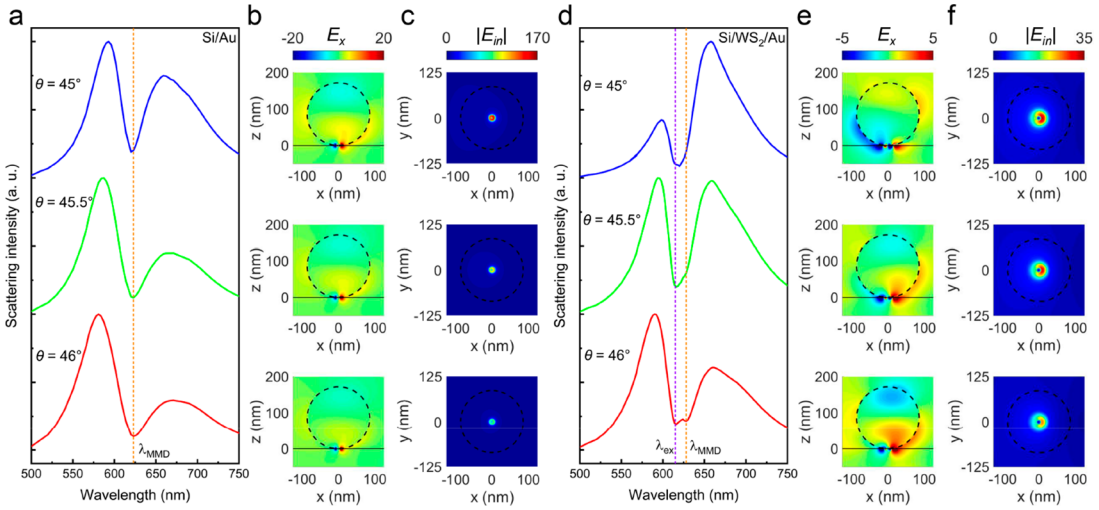

Figure 3. (a) Scattering spectra calculated for a Si/Au nanocavity (d = 172 nm) at different incidence angles of 45, 45.5, and 46°. The electric field distributions calculated at the Fano dip (624 nm) in the xz (E_x) and xy (E_{in}) planes are presented in (b) and (c), respectively. (d) Scattering spectra calculated for a Si/WS_2/Au nanocavity (d = 172 nm) at different incidence angles of 45, 45.5, and 46°. The electric field distributions calculated at the MMD resonance in the xz (E_x) and xy (E_{in}) planes are presented in (e) and (f), respectively.

RESULTS

The experimental setup used in this work is illustrated in Figure 1a (see Figure S2 in the Supporting Information). A p-polarized light with an incident angle of θ was used to excite the SPP on the Au film. The forward scattering of the Si nanoparticle was collected by a microscope and analyzed by a spectrometer. In Figure 1b, we show the optical images of WS_2 monolayers attached on the Au film. The optical quality and monolayer nature of the WS_2 flakes were examined by using scanning electron microscopy (SEM), photoluminescence (PL), and Raman scattering measurements (see Figure S3 in the Supporting Information).[47,48] Spherical Si nanoparticles fabricated by using femtosecond laser ablation were used to construct Si/Au nanocavities. The SEM image of a typical Si nanoparticle is shown in Figure 1c.

When $\theta < \theta_c \approx 43°$ (θ_c is the critical angle for total internal reflection), no SPP is generated and the Si nanoparticle is excited by the transmitted light, as shown in Figure 1d. In this case, the scattering of the Si nanoparticle arises from the mirror-image-induced magnetic dipole (MMD) originating from the ED and its mirror image induced by the Au film, which exhibits a scattering peak with reduced line width in the forward scattering spectrum of the Si nanoparticle.[39,49−52]

In Figure 2a, we present the scattering spectra simulated and measured for a Si/Au (upper panel) and a Si/WS_2/Au (lower panel) nanocavity in the case of $\theta < \theta_c$ (see Figure S4 in the Supporting Information). For the Si/Au nanocavity, one can identify four optical resonances originating from the coherent interaction among the Mie resonances (MD, ED, MQ, and EQ) of the Si nanoparticle with their mirror images induced by the Au film.[49−51] The measured spectrum is in qualitative agreement with the simulated spectrum. The scattering peak observed at ∼550 nm in the simulated spectra appears at ∼520 nm in the measured spectra. The discrepancy between them is caused mainly by the incident angle of the illumination light, the collection angle of the scattering light, and the smaller quantum efficiencies of the detector at short and long wavelengths. A similar situation is found for the Si/WS_2/Au nanocavity except for the splitting of the MMD due to the introduction of the WS_2 monolayer. By the choice of a Si nanoparticle with a diameter of $d \approx 175$ nm, the resonant wavelength of the MMD can be tuned to the exciton resonance of the WS_2 monolayer (615 nm), as shown in Figure 2a (upper panel). When a WS_2 monolayer is inserted into the nanocavity, the single scattering peak is split into two peaks due to the plasmon−exciton coupling, as shown in Figure 2a (lower panel). Unfortunately, the energy splitting in this case is not sufficient to satisfy the criterion for strong coupling.[39] In Figure 2b,c, we present the electric (E_x) and magnetic (H_y) field distributions simulated for the Si/Au (upper panel) and Si/WS_2/Au (lower panel) nanocavities at the exciton resonance (615 nm). Apart from the reduction in the field intensity, the electric and magnetic field distributions remain nearly unchanged after inserting the WS_2 monolayer. Since the excitons in the WS_2 monolayer are oriented mainly in the xy plane, they are coupled only with the in-plane electric field (i.e., $|E_{xy}| = (E_x^2 + E_y^2)^{1/2}$), which is presented in Figure 2d. It is notid that $|E_{xy}|$ is dramatically attenuated after inserting the WS_2 monolayer.

When $\theta > \theta_c$, the SPP will be generated and its interaction with the MMD results in a Fano dip.[42] In addition, the Fano line shape, which is characterized by the asymmetry parameter q, can be modified by simply varying the incident angle (see Figure S5 in the Supporting Information). For the Si/Au nanocavity shown in Figure 3a (d = 172 nm), the Fano dip appears at ∼624 nm. The corresponding electric field distributions in the xz and xy planes are shown in Figure 3b,c. It can be seen that the largest enhancement of $|E_{xy}|$ is achieved at θ = 45°, where the line shape of the Fano resonance appears to be symmetric. In this case, an enhancement factor as large as ∼170 is obtained. A rapid decrease of the enhancement factor is observed with an increase in the incident angle. If we inspect the distribution of $|E_{xy}|$, a ring-shaped pattern is observed. In addition, the intensity distribution is almost symmetric with respect to the y axis for θ = 45°. However, the intensity distribution becomes asymmetric with increasing incident angle, in accordance with the asymmetric Fano line shape.

In Figure 3d, we show the scattering spectra calculated for a Si/WS_2/Au nanocavity (d = 172 nm) at different incident

https://doi.org/10.1021/acs.nanolett.1c03576
Nano Lett. 2022, 22, 220−228

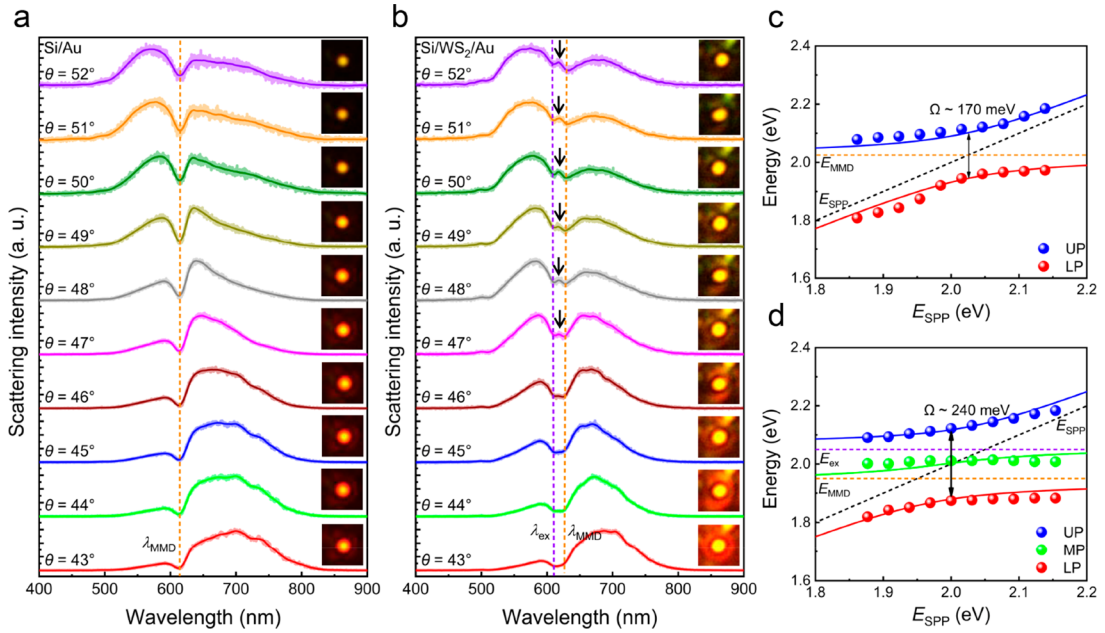

Figure 4. (a) Angle-resolved scattering spectra measured for a Si/Au nanocavity ($d \approx 169$ nm). The CCD images of the scattering light are shown as insets. The Fano dip, which corresponds to the MMD, is indicated by a dashed line. (b) Angle-resolved scattering spectra measured for a Si/WS_2/Au nanocavity ($d \approx 172$ nm). The CCD images of the scattering light are shown as insets. The resonant wavelengths of the exciton and MMD are indicated by dashed lines. (c) UP and LP branches (solid symbols) extracted from the scattering spectra shown in (a). The fittings of the UP and LP branches are represented by solid curves. The resonant energies of the SPP and MMD are indicated by dashed lines. (d) UP, MP, and LP branches (solid symbols) extracted from the scattering spectra shown in (b). The fittings of the UP, MP, and LP branches are represented by solid curves. The resonant energies of the SPP, MMD, and exciton are indicated by dashed lines.

angles. It is noted that the scattering spectra are modified after inserting the WS_2 monolayer. First, a small scattering peak emerges between the two large peaks, leading to two scattering valleys. This feature is clearly identified in the scattering spectrum obtained at $\theta = 46°$. A close inspection reveals that the two scattering valleys appear at the resonant wavelengths of the exciton (~615 nm) and the MMD (~626 nm). Similar to the coupling of the SPP and the MMD that leads to the formation of the Fano resonance, the modification in the scattering spectrum of the Si nanoparticle originates from the coupling of the SPP, the MMD, and the exciton modes. Three peaks observed in the scattering spectra can be attributed to the upper, middle, and lower polaritons. Second, the intensity of the scattering peak at the long wavelength is decreased with increasing incident angle. As a result, one can see the reversal of q from a negative to a positive value. Finally, the resonant wavelength of the MMD is red-shifted to 626 nm due to the introduction of the WS_2 monolayer (for a detailed comparison, see Figure S6 in the Supporting Information). We also examined the angle-resolved absorption spectra of the Si/WS_2/Au nanocavity and found that they are quite similar to the scattering spectra (Figure S7 in the Supporting Information).

In Figure 3e,f, we present the electric field distributions in the xz and xy planes calculated for the Si/WS_2/Au nanocavity at the MMD (626 nm). It is found that the enhancement factor for $|E_{xy}|$ is greatly reduced from ~170 to ~35 after inserting the WS_2 monolayer, which is caused by the energy transfer from the nanocavity to the excitons. Meanwhile, it is noted that the diameter of the ring-shaped intensity distribution is dramatically increased from ~20 to ~59 nm. Moreover, the field intensity distributions appear to be asymmetric in all cases.

In Figure 4a,b, we present the angle-resolved scattering spectra measured for a Si/Au and a Si/WS_2/Au nanocavity. For the Si/Au nanocavity, a Fano resonance is observed for each incident angle. Since the MMD is fixed at ~615 nm while the SPP is varied, the Fano line shape is modified when the incident angle is changed. In Figure 4c, we present dependences of the resonant energies of the hybrid states on the resonant energy of the SPP extracted from the angle-resolved scattering spectra of the Si/Au nanocavity, which clearly exhibits an anticrossing behavior. On the basis of the coupled harmonic oscillator model, the anticrossing behavior can be fitted by using a Hamiltonian with two eigenvalues:

$$\hat{H} = \hbar \begin{pmatrix} E_{SPP} - i\dfrac{\gamma_{SPP}}{2} & g_{SPP-MMD} \\ g_{SPP-MMD} & E_{MMD} - i\dfrac{\gamma_{MMD}}{2} \end{pmatrix} \quad (1)$$

Here, E_{SPP} and E_{MMD} are the resonant energies of the uncoupled SPP and MMD modes, respectively, γ_{SPP} and γ_{MMD} are the corresponding dissipation rates, and $g_{SPP-MMD}$ is the coupling strength between them. In Figure 4c, the fitting results are shown by two solid curves, which represent the dispersion relations of the two hybrid states. The energy splitting is derived to be $\Omega = 2g_{SPP-MMD} \approx 170$ meV. Since $\gamma_{SPP} \approx 220$ meV and $\gamma_{MMD} \approx 89$ meV, the criterion for strong coupling $\Omega > (\gamma_{SPP} + \gamma_{MMD})/2$ is satisfied.[11]

In the angle-resolved scattering spectra of the Si/WS_2/Au nanocavity (Figure 4b), a small scattering peak emerges between the two original peaks, as indicated by an arrow. Still, the resonant energies of the MMD and the exciton remain unchanged while that of the SPP is changed with the incident angle. Their coupling leads to the formation of three hybrid

https://doi.org/10.1021/acs.nanolett.1c03576
Nano Lett. 2022, 22, 220−228

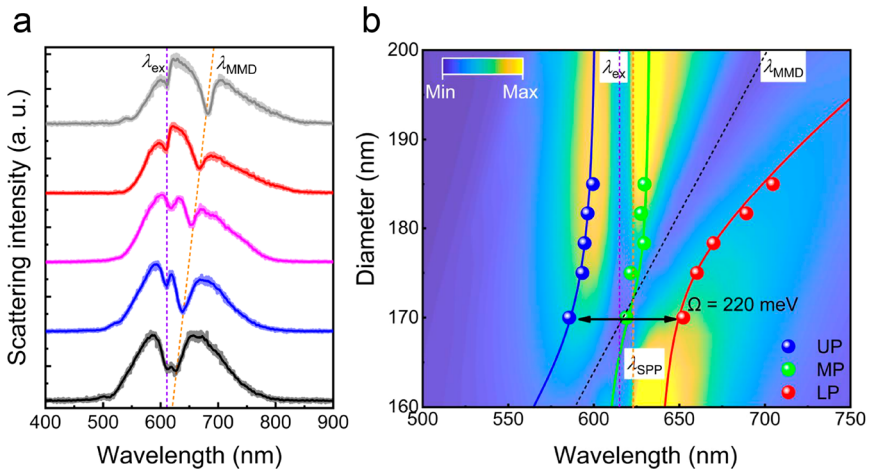

Figure 5. (a) Scattering spectra measured for Si/WS_2/Au hybrid nanocavities composed of Si nanoparticles with different diameters at an incidence angle of 47°. (b) Two-dimensional scattering spectra simulated for Si/WS_2/Au hybrid nanocavities composed of Si nanoparticles with different diameters. The two vertical dashed lines indicate the resonant wavelengths of the SPP and the exciton. The inclined dashed line indicates the evolution of the MMD with increasing diameter of the Si nanoparticle. The solid symbols are the experimental data extracted from the scattering spectra shown in (a). The solid curves represent the fittings of the UP, MP, and LP branches by using the coupled harmonic oscillator model with three oscillators (i.e., the SPP, the MMD, and the exciton).

states, whose resonant energies can be extracted from the wavelengths of the scattering peaks, as shown in Figure 4d. Similarly, the dispersions of the three hybrid states can be fitted by using a Hamiltonian with three eigenvalues:

$$\hat{H} = \hbar \begin{pmatrix} E_{SPP} - i\frac{\gamma_{SPP}}{2} & g_{SPP-MMD} & g_{SPP-ex} \\ g_{SPP-MMD} & E_{MMD} - i\frac{\gamma_{MMD}}{2} & g_{MMD-ex} \\ g_{SPP-ex} & g_{MMD-ex} & E_{ex} - i\frac{\gamma_{ex}}{2} \end{pmatrix} \quad (2)$$

Here, E_{SPP}, E_{MMD}, and E_{ex} are the resonant energies of the uncoupled SPP, MMD, and exciton modes, respectively, γ_{SPP}, γ_{MMD}, and γ_{ex} are the corresponding dissipation rates, and $g_{SPP-MMD}$, g_{SPP-ex}, and g_{MMD-ex} are the coupling strengths between the two modes. Similarly to a two-oscillator system, the Rabi splitting for a three-oscillator system is defined as the energy difference between the lower plexciton (LP) and the upper plexciton (UP).[19,23,43,53] For θ = 47°, the LP and UP are observed at ~1.88 and ~2.12 eV, respectively, resulting in a giant Rabi splitting of $\Omega_{UP\text{-}LP} \approx 240$ meV. Previously, the two-oscillator systems involved in the hybrid nanocavity (i.e., SPP−MMD, SPP−exciton, and MMD−exciton coupling) have been independently investigated.[38,39,42] While SPP−exciton coupling was employed to realize strong plasmon−exciton coupling, MMD−exciton coupling was found to only approach the strong-coupling regime. In addition, SPP−MMD coupling was confirmed to enter the strong-coupling regime. Similar to the use of an external cavity for a plasmonic nanoparticle array on a TMDC monolayer,[19] the introduction of SPP−MMD coupling into the hybrid nanocavity (i.e., the formation of the dark mode) makes it possible to greatly enhance the plasmon−exciton coupling. It is remarkable that the Rabi splitting observed in the three-oscillator system (SPP−MMD−exciton) is much larger than that in any of the two-oscillator systems (i.e., SPP−MMD (~170 meV), SPP−exciton (~102 meV), and MMD−exciton (~80 meV)).[38,39] To the best of our knowledge, the Rabi splitting observed in the hybrid nanocavity exceeds all the values reported previously for plasmonic nanocavities in air ambient conditions (Note 8 in the Supporting Information).[21,23,24,27−29] In Figure 4d, it is noted that the UP and LP bands change dramatically with the energy of SPP, while the MP band remains nearly unchanged. Since the coupling between the MMD and the exciton is not sensitive to the variation of the SPP, the energy splitting is assumed to be a constant (~80 meV). The coupling of the SPP with the exciton and the MMD results in two anticrossings at E_{ex} = 2.05 eV and E_{MMD} = 1.95 eV, respectively. The corresponding coupling strengths are estimated to be g_{MMD-ex} = 51 meV and $g_{SPP-MMD}$ = 98 meV, respectively.

For a three-oscillator system, the criterion for strong coupling can be written as[43]

$$\Omega > W_{UP}\gamma_{UP} + W_{MP}\gamma_{MP} + W_{LP}\gamma_{LP} \quad (3)$$

where W_{UP}, W_{MP}, and W_{LP} are the weights of UP, MP, and LP branches in the system, respectively, and γ_{UP}, γ_{MP}, and γ_{MP} are the line widths of the three branches (Note 9 in the Supporting Information). In our case, the strong coupling criteron for the SPP, the MMD, and the exciton modes can be expressed as

$$\Omega > 35\%\ \gamma_{SPP} + 37\%\ \gamma_{MMD} + 28\%\ \gamma_{ex} \quad (4)$$

where γ_{SPP} = 220 meV, γ_{MMD} = 89 meV, and γ_{ex} = 33 meV are the corresponding line widths. Apparently, the criterion for strong coupling is satisfied with $\Omega \approx 240$ meV (Notes 9 and 10 in the Supporting Information). For the Si/WS_2/Au nanocavity, the UP branch is mainly formed by the coupling of the SPP and the exciton. Similarly, the MP branch is dominated by the MMD and the exciton while the LP branch is composed of the SPP and the MMD.

Apart from the angle-resolved scattering spectra, one can also characterize the SPP−MMD−exciton coupling by changing the resonant energy of the MMD. In experiments, we measured the scattering spectra of five Si/WS_2/Au nanocavities constructed by using Si nanoparticles with different diameters at θ = 47°, as shown in Figure 5a. In each case, one can clearly identify three scattering peaks representing the resonant wavelengths of the three hybrid

https://doi.org/10.1021/acs.nanolett.1c03576
Nano Lett. 2022, 22, 220−228

states and two scattering valleys corresponding to the resonant wavelengths of the exciton and the MMD. It is remarkable that the resonant wavelength of the exciton remains unchanged at ~615 nm, while that of the MMD is changed. In Figure 5b, we present the two-dimensional scattering spectra simulated for $Si/WS_2/Au$ nanocavities containing Si nanoparticles with different diameters. One can reveal three plexciton bands that can be well described by using a Hamiltonian with three eigenvalues (i.e., eq 2). In Figure 5b, the resonant energies of the three plexciton states as a function of the resonant energy of the MMD extracted from the scattering spectra in Figure 5a are shown. An excellent agreement between the experimental data and the simulation results is observed. The Rabi splitting derived from the fitting result is ~220 meV, which is close to the value obtained by using angle-resolved scattering spectra. In addition, the criterion for strong coupling is also fulfilled.

We also examined the photoluminescence (PL) from $Si/WS_2/Au$ nanocavities and compared it with that from the WS_2 monolayer on the Au film (Figure S11 in the Supporting Information). In this case, the laser spot size (a few micrometers) is much larger than the diameters of Si nanoparticles and the PL comes mainly from the area of the WS_2 monolayer that does not couple with the nanocavities. However, a reduction in the PL intensity originating from the strong plasmon−exciton coupling was still observed for the $Si/WS_2/Au$ nanocavities, in good agreement with previous observations.[30,54,55]

CONCLUSION

In summary, we have proposed a novel strategy to realize SPP−MMD−exciton polaritons in a dielectric−metal hybrid nanocavity composed of a dielectric nanoparticle (Si) and a metal film (Au) with an embedded two-dimensional material (WS_2 monolayer). The new findings and insights of this work include (1) the dielectric−metal hybrid nanocavities composed of Si nanoparticles and an Au film support "dark" modes with a large enhancement factor, leading to a giant energy splitting of ~240 meV; (2) the first demonstration of the strong coupling among three excitations by exploiting dielectric−metal hybrid nanocavities is first demonstrated; (3) the plasmon−exciton coupling is revealed in both angle- and size-resolved scattering spectra, providing more degrees for manipulating the coupling strength. Our findings pave the way for realizing strong coupling between plasmons and excitons in dielectric−metal hybrid systems and open new horizons for constructing nanoscale photonic devices.

METHODS

Sample Preparation. The WS_2 monolayers used in this work were first synthesized on a Si substrate via chemical vapor deposition method and then transferred to an Au/SiO_2 substrate with a 50 nm thick Au film. Spherical Si nanoparticles with different diameters were fabricated by using femtosecond laser ablation.[56] The 800 nm femtosecond laser pulses (Legend. Coherent) with a duration of 100 fs and a repetition rate of 1 kHz was employed to ablate the Si wafer immersed in deionized water. The aqueous solution of Si nanoparticles was dropped and dried on WS_2 monolayers attached on the Au/SiO_2 substrate, giving $Si/WS_2/Au$ nanocavities operating at different wavelength.

It was confirmed by the combination of transmission electric microscopy (TEM), scattering spectra measurements, and numerical simulations that the prepared Si nanoparticles are crystalline.[57] Although Si nanoparticles with different sizes were randomly distributed on the WS_2 monolayer, we could easily find Si nanoparticles with suitable diameters for the construction of nanocavities on the basis of their forward scattering spectra, which can be easily obtained by using conventional dark-field microscopy.[49]

Optical Characterization. A home-built coupling system was used to generate the SPP on the surface of the Au film via the K-R configuration, which was employed to excite Si/Au and $Si/WS_2/Au$ nanocavities, as schematically shown in Figure 1a. Collimated *p*-polarized white light delivered by a multimode optical fiber was used as the excitation source. The incident angle of the excitation light could be easily adjusted. The scattering light of Si/Au and $Si/WS_2/Au$ nanocavities was collected by using the objective (100×, NA = 0.85) of a dark-field microscope (Axio Observer A1, Zeiss) for analysis and imaging. The scattering spectra were analyzed by using a spectrometer (SR-5001-B1, Andor), and the images of scattering light were recorded by using a color charge coupled device (CCD) (DS-Ri2, Nikon).

Characterization of WS_2 Monolayer. The morphologies of WS_2 monolayers were examined by using a bright-field microscope and a scanning electron microscope (SEM) (UItra55, Zeiss). The photoluminescence and Raman spectra of WS_2 monolayers were measured by using a 532 nm laser and a Renishaw inVia Reflex system, respectively. The laser power used for the spectral measurements was chosen to be 1.0 mW.

Numerical Simulations. In this work, the numerical simulations were carried out by using the finite-difference time-domain (FDTD) technique. The dielectric constants of Au and Si were taken from Johnson and Christy[58] and from Palik,[59] respectively. The dielectric constant of a WS_2 monolayer was obtained from previous literature.[6] The exciton energy in WS_2 monolayer is 2.02 eV. The refractive indices of the prism and the surrounding environment were set to be 1.5 and 1.0, respectively. In the calculation, the thickness of the WS_2 monolayer was chosen to be 1.0 nm. The smallest mesh size was chosen to be 0.5 nm, which was used in the gap region between the nanoparticle and the film.

ASSOCIATED CONTENT

Supporting Information

The Supporting Information is available free of charge at https://pubs.acs.org/doi/10.1021/acs.nanolett.1c03576.

Detailed information about the morphology and optical characterization of monolayer WS_2 and hybrid nanocavities, optical properties of hybrid nanocavities, angle-resolved absorption spectra, mode hybridization analysis, and a comparison of different configurations/materials (PDF)

AUTHOR INFORMATION

Corresponding Author

Sheng Lan − *Guangdong Provincial Key Laboratory of Nanophotonic Functional Materials and Devices, School of Information and Optoelectronic Science and Engineering, South China Normal University, Guangzhou 510006, People's Republic of China;* orcid.org/0000-0002-7277-0042; Email: slan@scnu.edu.cn

https://doi.org/10.1021/acs.nanolett.1c03576
Nano Lett. 2022, 22, 220−228

Authors

Fu Deng − *Guangdong Provincial Key Laboratory of Nanophotonic Functional Materials and Devices, School of Information and Optoelectronic Science and Engineering, South China Normal University, Guangzhou 510006, People's Republic of China*

Hongxin Huang − *Guangdong Provincial Key Laboratory of Nanophotonic Functional Materials and Devices, School of Information and Optoelectronic Science and Engineering, South China Normal University, Guangzhou 510006, People's Republic of China;* orcid.org/0000-0002-0398-5365

Jing-Dong Chen − *College of Physics and Information Engineering, Minnan Normal University, Zhangzhou 363000, People's Republic of China;* orcid.org/0000-0003-3375-2869

Shimei Liu − *Guangdong Provincial Key Laboratory of Nanophotonic Functional Materials and Devices, School of Information and Optoelectronic Science and Engineering, South China Normal University, Guangzhou 510006, People's Republic of China*

Huajian Pang − *Guangdong Provincial Key Laboratory of Nanophotonic Functional Materials and Devices, School of Information and Optoelectronic Science and Engineering, South China Normal University, Guangzhou 510006, People's Republic of China*

Xiaobing He − *Guangdong Provincial Key Laboratory of Nanophotonic Functional Materials and Devices, School of Information and Optoelectronic Science and Engineering, South China Normal University, Guangzhou 510006, People's Republic of China*

Complete contact information is available at: https://pubs.acs.org/10.1021/acs.nanolett.1c03576

Author Contributions

§F.D. and H.H. contributed equally to this work.

Author Contributions

F.D., H.H., and S. Lan conceived the idea; H.H., S. Liu, H.P., and X.H. fabricated the samples; H.H. and S. Liu performed the measurements; F.D, H.H., and J.-D.C. carried out the numerical simulations; F.D. and H.H. analyzed the data; F.D., H.H., and S. Lan wrote the manuscript; S. Lan supervised the project. All of the authors read and commented on the manuscript.

Notes

The authors declare no competing financial interest.

■ ACKNOWLEDGMENTS

This work was financially supported by the National Natural Science Foundation of China (Grant Nos. 11874020 and 12174123).

■ REFERENCES

(1) Splendiani, A.; Sun, L.; Zhang, Y.; Li, T.; Kim, J.; Chim, C. Y.; Galli, G.; Wang, F. Emerging photoluminescence in monolayer MoS_2. *Nano Lett.* **2010**, *10* (4), 1271−1275.

(2) Mak, K. F.; Lee, C.; Hone, J.; Shan, J.; Heinz, T. F. Atomically thin MoS_2: a new direct-gap semiconductor. *Phys. Rev. Lett.* **2010**, *105* (13), 136805.

(3) Ye, Z.; Cao, T.; O'Brien, K.; Zhu, H.; Yin, X.; Wang, Y.; Louie, S. G.; Zhang, X. Probing excitonic dark states in single-layer tungsten disulphide. *Nature* **2014**, *513* (7517), 214−218.

(4) Chernikov, A.; Berkelbach, T. C.; Hill, H. M.; Rigosi, A.; Li, Y.; Aslan, O. B.; Reichman, D. R.; Hybertsen, M. S.; Heinz, T. F. Exciton binding energy and nonhydrogenic Rydberg series in monolayer WS_2. *Phys. Rev. Lett.* **2014**, *113* (7), 076802.

(5) He, K.; Kumar, N.; Zhao, L.; Wang, Z.; Mak, K. F.; Zhao, H.; Shan, J. Tightly bound excitons in monolayer WSe_2. *Phys. Rev. Lett.* **2014**, *113* (2), 026803.

(6) Li, Y.; Chernikov, A.; Zhang, X.; Rigosi, A.; Hill, H. M.; van der Zande, A. M.; Chenet, D. A.; Shih, E.-M.; Hone, J.; Heinz, T. F. Measurement of the optical dielectric function of monolayer transition-metal dichalcogenides:MoS_2, $MoSe_2$, WS_2, and WSe_2. *Phys. Rev. B* **2014**, *90* (20), 205422.

(7) Amani, M.; Taheri, P.; Addou, R.; Ahn, G. H.; Kiriya, D.; Lien, D. H.; Ager, J. W., 3rd; Wallace, R. M.; Javey, A. Recombination Kinetics and Effects of Superacid Treatment in Sulfur- and Selenium-Based Transition Metal Dichalcogenides. *Nano Lett.* **2016**, *16* (4), 2786−2791.

(8) Raimond, J. M.; Brune, M.; Haroche, S. Manipulating quantum entanglement with atoms and photons in a cavity. *Rev. Mod. Phys.* **2001**, *73* (3), 565−582.

(9) Khitrova, G.; Gibbs, H. M.; Kira, M.; Koch, S. W.; Scherer, A. Vacuum Rabi splitting in semiconductors. *Nat. Phys.* **2006**, *2* (2), 81−90.

(10) Smolka, S.; Wuester, W.; Haupt, F.; Faelt, S.; Wegscheider, W.; Imamoglu, A. Cavity quantum electrodynamics with many-body states of a two-dimensional electron gas. *Science* **2014**, *346* (6207), 332−335.

(11) Torma, P.; Barnes, W. L. Strong coupling between surface plasmon polaritons and emitters: a review. *Rep. Prog. Phys.* **2015**, *78* (1), 013901.

(12) Baranov, D. G.; Zuev, D. A.; Lepeshov, S. I.; Kotov, O. V.; Krasnok, A. E.; Evlyukhin, A. B.; Chichkov, B. N. All-dielectric nanophotonics: the quest for better materials and fabrication techniques. *Optica* **2017**, *4* (7), 814−825.

(13) Liu, R. M.; Zhou, Z. K.; Yu, Y. C.; Zhang, T. W.; Wang, H.; Liu, G. H.; Wei, Y. M.; Chen, H. J.; Wang, X. H. Strong Light-Matter Interactions in Single Open Plasmonic Nanocavities at the Quantum Optics Limit. *Phys. Rev. Lett.* **2017**, *118* (23), 237401.

(14) Chen, W.; Beck, K. M.; Bucker, R.; Gullans, M.; Lukin, M. D.; Tanji-Suzuki, H.; Vuletic, V. All-optical switch and transistor gated by one stored photon. *Science* **2013**, *341* (6147), 768−770.

(15) Sillanpää, M. A.; Park, J. I.; Simmonds, R. W. Coherent quantum state storage and transfer between two phase qubits via a resonant cavity. *Nature* **2007**, *449* (7161), 438−442.

(16) Ye, Y.; Wong, Z. J.; Lu, X.; Ni, X.; Zhu, H.; Chen, X.; Wang, Y.; Zhang, X. Monolayer excitonic laser. *Nat. Photonics* **2015**, *9* (11), 733−737.

(17) Wu, S.; Buckley, S.; Schaibley, J. R.; Feng, L.; Yan, J.; Mandrus, D. G.; Hatami, F.; Yao, W.; Vuckovic, J.; Majumdar, A.; Xu, X. Monolayer semiconductor nanocavity lasers with ultralow thresholds. *Nature* **2015**, *520* (7545), 69−72.

(18) Liu, X.; Galfsky, T.; Sun, Z.; Xia, F.; Lin, E.-c.; Lee, Y.-H.; Kéna-Cohen, S.; Menon, V. M. Strong light−matter coupling in two-dimensional atomic crystals. *Nat. Photonics* **2015**, *9* (1), 30−34.

(19) Bisht, A.; Cuadra, J.; Wersäll, M.; Canales, A.; Antosiewicz, T. J.; Shegai, T. Collective Strong Light-Matter Coupling in Hierarchical Microcavity-Plasmon-Exciton Systems. *Nano Lett.* **2019**, *19* (1), 189−196.

(20) Lee, B.; Liu, W.; Naylor, C. H.; Park, J.; Malek, S. C.; Berger, J. S.; Johnson, A. T. C.; Agarwal, R. Electrical Tuning of Exciton-Plasmon Polariton Coupling in Monolayer MoS_2 Integrated with Plasmonic Nanoantenna Lattice. *Nano Lett.* **2017**, *17* (7), 4541−4547.

(21) Wen, J.; Wang, H.; Wang, W.; Deng, Z.; Zhuang, C.; Zhang, Y.; Liu, F.; She, J.; Chen, J.; Chen, H.; Deng, S.; Xu, N. Room-Temperature Strong Light-Matter Interaction with Active Control in Single Plasmonic Nanorod Coupled with Two-Dimensional Atomic Crystals. *Nano Lett.* **2017**, *17* (8), 4689−4697.

(22) Zheng, D.; Zhang, S.; Deng, Q.; Kang, M.; Nordlander, P.; Xu, H. Manipulating Coherent Plasmon-Exciton Interaction in a Single Silver Nanorod on Monolayer WSe_2. *Nano Lett.* **2017**, *17* (6), 3809−3814.
(23) Cuadra, J.; Baranov, D. G.; Wersall, M.; Verre, R.; Antosiewicz, T. J.; Shegai, T. Observation of Tunable Charged Exciton Polaritons in Hybrid Monolayer WS_2-Plasmonic Nanoantenna System. *Nano Lett.* **2018**, *18* (3), 1777−1785.
(24) Munkhbat, B.; Baranov, D. G.; Bisht, A.; Hoque, M. A.; Karpiak, B.; Dash, S. P.; Shegai, T. Electrical Control of Hybrid Monolayer Tungsten Disulfide-Plasmonic Nanoantenna Light-Matter States at Cryogenic and Room Temperatures. *ACS Nano* **2020**, *14* (1), 1196−1206.
(25) Stuhrenberg, M.; Munkhbat, B.; Baranov, D. G.; Cuadra, J.; Yankovich, A. B.; Antosiewicz, T. J.; Olsson, E.; Shegai, T. Strong Light-Matter Coupling between Plasmons in Individual Gold Bi-pyramids and Excitons in Mono- and Multilayer WSe_2. *Nano Lett.* **2018**, *18* (9), 5938−5945.
(26) Geisler, M.; Cui, X.; Wang, J.; Rindzevicius, T.; Gammelgaard, L.; Jessen, B. S.; Gonçalves, P. A. D.; Todisco, F.; Bøggild, P.; Boisen, A.; Wubs, M.; Mortensen, N. A.; Xiao, S.; Stenger, N. Single-Crystalline Gold Nanodisks on WS_2 Mono- and Multilayers for Strong Coupling at Room Temperature. *ACS Photonics* **2019**, *6* (4), 994−1001.
(27) Han, X.; Wang, K.; Xing, X.; Wang, M.; Lu, P. Rabi Splitting in a Plasmonic Nanocavity Coupled to a WS_2 Monolayer at Room Temperature. *ACS Photonics* **2018**, *5* (10), 3970−3976.
(28) Kleemann, M. E.; Chikkaraddy, R.; Alexeev, E. M.; Kos, D.; Carnegie, C.; Deacon, W.; de Pury, A. C.; Grosse, C.; de Nijs, B.; Mertens, J.; Tartakovskii, A. I.; Baumberg, J. J. Strong-coupling of WSe_2 in ultra-compact plasmonic nanocavities at room temperature. *Nat. Commun.* **2017**, *8* (1), 1296.
(29) Qin, J.; Chen, Y. H.; Zhang, Z.; Zhang, Y.; Blaikie, R. J.; Ding, B.; Qiu, M. Revealing Strong Plasmon-Exciton Coupling between Nanogap Resonators and Two-Dimensional Semiconductors at Ambient Conditions. *Phys. Rev. Lett.* **2020**, *124* (6), 063902.
(30) Jiang, Y.; Wang, H.; Wen, S.; Chen, H.; Deng, S. Resonance Coupling in an Individual Gold Nanorod-Monolayer WS_2 Heterostructure: Photoluminescence Enhancement with Spectral Broadening. *ACS Nano* **2020**, *14* (10), 13841−13851.
(31) Zhang, W.; You, J. B.; Liu, J.; Xiong, X.; Li, Z.; Png, C. E.; Wu, L.; Qiu, C. W.; Zhou, Z. K. Steering Room-Temperature Plexcitonic Strong Coupling: A Diexcitonic Perspective. *Nano Lett.* **2021**, *21*, 8979−8986.
(32) Wang, M.; Krasnok, A.; Zhang, T.; Scarabelli, L.; Liu, H.; Wu, Z.; Liz-Marzan, L. M.; Terrones, M.; Alu, A.; Zheng, Y. Tunable Fano Resonance and Plasmon-Exciton Coupling in Single Au Nanotriangles on Monolayer WS_2 at Room Temperature. *Adv. Mater.* **2018**, *30* (22), No. 1705779.
(33) Lo, T. W.; Zhang, Q.; Qiu, M.; Guo, X.; Meng, Y.; Zhu, Y.; Xiao, J. J.; Jin, W.; Leung, C. W.; Lei, D. Thermal Redistribution of Exciton Population in Monolayer Transition Metal Dichalcogenides Probed with Plasmon-Exciton Coupling Spectroscopy. *ACS Photonics* **2019**, *6* (2), 411−421.
(34) Lepeshov, S.; Wang, M.; Krasnok, A.; Kotov, O.; Zhang, T.; Liu, H.; Jiang, T.; Korgel, B.; Terrones, M.; Zheng, Y.; Alu, A. Tunable Resonance Coupling in Single Si Nanoparticle-Monolayer WS_2 Structures. *ACS Appl. Mater.& Interfaces* **2018**, *10* (19), 16690−16697.
(35) Wang, H.; Wen, J.; Wang, W.; Xu, N.; Liu, P.; Yan, J.; Chen, H.; Deng, S. Resonance Coupling in Heterostructures Composed of Silicon Nanosphere and Monolayer WS_2: A Magnetic-Dipole-Mediated Energy Transfer Process. *ACS Nano* **2019**, *13* (2), 1739−1750.
(36) Li, G. C.; Zhang, Q.; Maier, S. A.; Lei, D. Plasmonic particle-on-film nanocavities: a versatile platform for plasmon-enhanced spectroscopy and photochemistry. *Nanophotonics* **2018**, *7* (12), 1865−1889.
(37) Chen, J. D.; Xiang, J.; Jiang, S.; Dai, Q. F.; Tie, S. L.; Lan, S. Radiation of the high-order plasmonic modes of large gold nanospheres excited by surface plasmon polaritons. *Nanoscale* **2018**, *10* (19), 9153−9163.
(38) Deng, F.; Liu, H.; Xu, L.; Lan, S.; Miroshnichenko, A. E. Strong Exciton−Plasmon Coupling in a WS_2 Monolayer on Au Film Hybrid Structures Mediated by Liquid Ga Nanoparticles. *Laser & Photonics Rev.* **2020**, *14* (4), 1900420.
(39) Huang, H.; Deng, F.; Xiang, J.; Li, S.; Lan, S. Plasmon-exciton coupling in dielectric-metal hybrid nanocavities with an embedded two-dimensional material. *Appl. Surf. Sci.* **2021**, *542*, 148660.
(40) Kuznetsov, A. I.; Miroshnichenko, A. E.; Fu, Y. H.; Zhang, J.; Luk'yanchuk, B. Magnetic light. *Sci. Rep.* **2012**, *2*, 492.
(41) Kuznetsov, A. I.; Miroshnichenko, A. E.; Brongersma, M. L.; Kivshar, Y. S.; Luk'yanchuk, B. Optically resonant dielectric nanostructures. *Science* **2016**, *354* (6314), 1.
(42) Xiang, J.; Chen, J.; Lan, S.; Miroshnichenko, A. E. Nanoscale Optical Display and Sensing Based on the Modification of Fano Lineshape. *Adv. Opt. Mater.* **2020**, *8* (16), 2000489.
(43) Li, B. W.; Zu, S.; Zhang, Z. P.; Zheng, L. H.; Jiang, Q.; Du, B. W.; Luo, Y.; Gong, Y. J.; Zhang, Y. F.; Lin, F.; Shen, B.; Zhu, X.; Ajayan, P. M.; Fang, Z. Y. Large Rabi splitting obtained in Ag-WS_2 strong-coupling heterostructure with optical microcavity at room temperature. *Opto-Electronic Advances* **2019**, *2* (5), 19000801.
(44) Rousseaux, B.; Baranov, D. G.; Antosiewicz, T. J.; Shegai, T.; Johansson, G. Strong coupling as an interplay of quantum emitter hybridization with plasmonic dark and bright modes. *ACS Appl. Mater.& Interfaces* **2020**, *2* (3), 033056.
(45) Verre, R.; Baranov, D. G.; Munkhbat, B.; Cuadra, J.; Kall, M.; Shegai, T. Transition metal dichalcogenide nanodisks as high-index dielectric Mie nanoresonators. *Nat. Nanotechnol.* **2019**, *14* (7), 679−683.
(46) Monticone, F.; Sounas, D.; Krasnok, A.; Alù, A. Can a Nonradiating Mode Be Externally Excited? Nonscattering States versus Embedded Eigenstates. *ACS Photonics* **2019**, *6* (12), 3108−3114.
(47) Ovchinnikov, D.; Allain, A.; Huang, Y. S.; Dumcenco, D.; Kis, A. Electrical transport properties of single-layer WS_2. *ACS Nano* **2014**, *8* (8), 8174−8181.
(48) Gutiérrez, H. R.; Perea-López, N.; Elías, A. L.; Berkdemir, A.; Wang, B.; Lv, R.; López-Urías, F.; Crespi, V. H.; Terrones, H.; Terrones, M. Extraordinary Room-Temperature Photoluminescence in Triangular WS_2 Monolayers. *Nano Lett.* **2013**, *13* (8), 3447−3454.
(49) Li, H.; Xu, Y.; Xiang, J.; Li, X. F.; Zhang, C. Y.; Tie, S. L.; Lan, S. Exploiting the interaction between a semiconductor nanosphere and a thin metal film for nanoscale plasmonic devices. *Nanoscale* **2016**, *8* (45), 18963−18971.
(50) Miroshnichenko, A. E.; Evlyukhin, A. B.; Kivshar, Y. S.; Chichkov, B. N. Substrate-Induced Resonant Magnetoelectric Effects for Dielectric Nanoparticles. *ACS Photonics* **2015**, *2* (10), 1423−1428.
(51) Huang, Z.; Wang, J.; Liu, Z.; Xu, G.; Fan, Y.; Zhong, H.; Cao, B.; Wang, C.; Xu, K. Strong-Field-Enhanced Spectroscopy in Silicon Nanoparticle Electric and Magnetic Dipole Resonance near a Metal Surface. *J. Phys. Chem. C* **2015**, *119* (50), 28127−28135.
(52) Sinev, I.; Iorsh, I.; Bogdanov, A.; Permyakov, D.; Komissarenko, F.; Mukhin, I.; Samusev, A.; Valuckas, V.; Kuznetsov, A. I.; Luk'yanchuk, B. S.; Miroshnichenko, A. E.; Kivshar, Y. S. Polarization control over electric and magnetic dipole resonances of dielectric nanoparticles on metallic films. *Laser & Photonics Rev.* **2016**, *10* (5), 799−806.
(53) As' ham, K.; Al-Ani, I.; Huang, L.; Miroshnichenko, A. E.; Hattori, H. T. J. A. P. Boosting strong coupling in a hybrid WSe_2 monolayer−anapole−plasmon system. *ACS Photonics* **2021**, *8* (2), 489−496.
(54) Qi, X.; Lo, T. W.; Liu, D.; Feng, L.; Chen, Y.; Wu, Y.; Ren, H.; Guo, G.-C.; Lei, D.; Ren, X. Effects of gap thickness and emitter location on the photoluminescence enhancement of monolayer MoS_2 in a plasmonic nanoparticle-film coupled system. *Nanophotonics* **2020**, *9* (7), 2097−2105.

https://doi.org/10.1021/acs.nanolett.1c03576
Nano Lett. 2022, 22, 220−228

(55) Choi, S. Y.; Yip, C. T.; Li, G.-C.; Lei, D. Y.; Fung, K. H.; Yu, S. F.; Hao, J. Photoluminescence enhancement in few-layer WS_2 films via Au nanoparticles. *AIP Advances* **2015**, *5* (6), 067148.
(56) Li, C.-Q.; Zhang, C.-Y.; Huang, Z.-S.; Li, X.-F.; Dai, Q.-F.; Lan, S.; Tie, S.-L. Assembling of Silicon Nanoflowers with Significantly Enhanced Second Harmonic Generation Using Silicon Nanospheres Fabricated by Femtosecond Laser Ablation. *J. Phys. Chem. C* **2013**, *117* (46), 24625−24631.
(57) Zhang, C.; Xu, Y.; Liu, J.; Li, J.; Xiang, J.; Li, H.; Li, J.; Dai, Q.; Lan, S.; Miroshnichenko, A. E. Lighting up silicon nanoparticles with Mie resonances. *Nat. Commun.* **2018**, *9* (1), 2964.
(58) Johnson, P. B.; Christy, R. W. Optical Constants of the Noble Metals. *Phys. Rev. B* **1972**, *6* (12), 4370−4379.
(59) Palik, E. D. *Handbook of optical constants of solids*; Academic Press: 1998; Vol. 3.

https://doi.org/10.1021/acs.nanolett.1c03576
Nano Lett. 2022, 22, 220−228